

Understanding small neutrino mass and its implication

Hsiang-nan Li

Institute of Physics, Academia Sinica, Taipei, Taiwan 115, Republic of China

(Dated: April 26, 2024)

We have derived previously the relations between the neutrino masses and mixing angles in a dispersive analysis on the mixing of neutral leptonic states. The only involved assumption is that the electroweak symmetry of the Standard Model (SM) is restored at a high energy scale in some new physics scenario, which diminishes the box diagrams responsible for the mixing. Here we include corrections to the analysis up to three loops, arising from exchanges of additional neutral and charged scalars in the electroweak symmetric phase. The solution to the dispersion relation for the $\mu^-e^+-\mu^+e^-$ mixing generates a typical neutrino mass $m_\nu \sim O(1)$ eV in the SM unambiguously. The solution also favors the normal ordering of the neutrino masses over the inverted one, and links the large electroweak symmetry restoration, i.e., new physics scale to the small neutrino mass.

I. INTRODUCTION

It has been a long pursuit in particle physics to understand the flavor structure of the Standard Model (SM). We proposed recently [1–3] that analyticity imposes additional dynamical constraints on the SM parameters beyond the Lagrangian level, which can account for the mass hierarchy and the distinct mixing patterns between quarks and leptons. Take the mixing of the neutral leptonic states μ^-e^+ and μ^+e^- as an example, where the muon is treated as being heavy with the invariant mass squared s , and the electron is regarded as being massless. The mixing amplitude governed by the leading-order (LO) box diagrams must respect a dispersion relation formulated in the s complex plane. It was argued that the mixing phenomenon will disappear, if the electroweak symmetry of the SM is restored at a high energy scale Λ [4, 5]. The composite Higgs model described in [6] provides a suitable platform for the argumentation; the electroweak group in their model is broken at a scale much lower than the condensate scale, implying the existence of a symmetric phase which we refer to. The disappearance of the mixing at $s > \Lambda^2$ was taken as the LO input to the dispersion relation, and the corresponding solution at low $s < \Lambda^2$, i.e., in the symmetry broken phase, was found to effectively bind the neutrino masses and the Pontecorvo–Maki–Nakagawa–Sakata (PMNS) matrix elements involved in the box diagrams.

Several important observations were extracted from the dispersive constraints on the neutrino masses and the PMNS matrix elements [1]. The neutrino mass ordering, whose various scenarios have not been discriminated experimentally, has remained unsettled in neutrino physics [7]. It was noticed that the neutrino masses in the normal ordering (NO), instead of in the inverted ordering (IO) or quasi-degenerate spectrum, match the observed PMNS matrix elements. The neutrino mixing angles larger than the quark ones were attributed to the inequality of the mass ratios, $m_2^2/m_3^2 \gg m_s^2/m_b^2$, where m_2 (m_3) is the second-generation (third-generation) neutrino mass and m_s (m_b) is the s (b) quark mass. The combination with the dispersive analysis of the $\tau^-e^+-\tau^+e^-$ mixing further demands unequivocally the mixing angle $\theta_{23} \approx 45^\circ$ in accordance with its measured value around the maximal mixing. We emphasize that the above observations are established without resorting to specific new ingredients beyond the SM (for recent endeavors on this topic, refer to [8–16]). The only required assumption is the restoration of the electroweak symmetry at a high energy scale. The successful explanation on part of the SM flavor structure thus also sheds light on potential new physics models.

Precisely speaking, our previous study explored the connection between the mixing angles and the ratios of the neutrino masses, instead of the absolute values of the neutrino masses [17]. Therefore, one of the key issues in neutrino physics, i.e., the smallness of the neutrino masses, has not been addressed. As a follow-up, we include loop corrections to the LO formalism, which arise from exchanges of additional neutral and charged scalars in the electroweak symmetric phase. The solution to the dispersion relation for the $\mu^-e^+-\mu^+e^-$ mixing with the high-energy inputs up to three loops generates a tiny neutrino mass scale in the SM via the equation

$$m_\nu^2 \sqrt{\ln \frac{m_W^2}{m_\nu^2}} \approx \frac{\sqrt{3}}{128\pi^2} \frac{m_\mu^2 m_e^2}{v^2}, \quad (1)$$

with the W boson mass m_W , the muon (electron) mass m_μ (m_e) and the vacuum expectation value (VEV) v of the Higgs field. Compared to the well-known seesaw mechanism [18], the VEV v plays the role of a heavy Majorana neutrino mass in suppressing neutrino masses relative to charged lepton masses. Equation (1) leads to $m_\nu \sim O(1)$ eV unambiguously, which, as an order-of-magnitude estimate, is compatible with the upper bound on the neutrino mass $m_\nu < 0.9$ eV at 90% CL from the the endpoint spectrum of the tritium β -decay measured by the KATRIN Collaboration [19].

We also find from the solution that the tiny neutrino mass hints a large electroweak symmetry restoration Λ through the order-of-magnitude formula

$$\ln \frac{\Lambda}{m_W} \sim O(1) \sqrt{\ln \frac{m_W^2}{m_\nu^2}}, \quad (2)$$

where $O(1)$ denotes a coefficient of order of unity. In other words, the small neutrino mass is indeed linked to a new physics scale [20]. As mentioned before, we have demonstrated [1] that the neutrino masses in the NO satisfies better the LO dispersive constraints from the mixing of neutral leptonic states, compared to the IO. We examine whether this postulation sustains its validity by deriving the constraint under the multi-loop input,

$$U_{\mu 1}^* U_{e 1} (m_3 - m_1) + U_{\mu 2}^* U_{e 2} (m_3 - m_2) = O\left(\frac{m_\nu^2}{v}\right) \approx 0, \quad (3)$$

with the PMNS matrix elements $U_{\mu i}$ and $U_{e i}$ and the first-generation neutrino mass m_1 . It will be shown that Eq. (3) confirms the preference on the fitted parameters associated with the NO. The discrimination is mainly due to the different CP phases determined for the two possible mass orderings.

The rest of the paper is organized as follows. We recapture our framework [1] in Sec. II, and present the real part of the mixing amplitude in the symmetric phase and the imaginary part in the broken phase. The two pieces are substituted into the dispersion relation respected by the mixing amplitude in Sec. III to construct the solution. Equations (1)-(3) are established, and their physical implications are elaborated. Section IV contains the conclusion and outlook. The real part of the mixing amplitude is evaluated up to three loops in the Appendix.

II. FORMALISM

Consider the mixing of the neutral leptonic states $\mathcal{L}_L^- \ell_L^+$ and $\mathcal{L}_L^+ \ell_L^-$, where \mathcal{L} (ℓ) stands for a massive (light) charged lepton and L labels the left-handedness. The right-handedness will be labeled by R below. Before the electroweak symmetry breaking, all particles are massless, and leptons are in their flavor eigenstates. The mixing occurs through exchanges of charged or neutral scalars among leptons, whose strengths are characterize by the Yukawa couplings. The Yukawa matrix elements are not all independent, so the discussion of the mixing in the symmetric phase will be more tedious, if it is based on the Yukawa matrices. A more transparent picture is attained by implementing the fermion field transformations adopted in the symmetry broken phase. The standard unitary transformation of fermion fields from the flavor eigenstates with the superscript f to the mass eigenstates reads

$$\nu_L^{(f)} = U_\nu \nu_L, \quad \nu_R^{(f)} = V_\nu \nu_R, \quad \ell_L^{(f)} = U_\ell \ell_L, \quad \ell_R^{(f)} = V_\ell \ell_R, \quad (4)$$

which diagonalizes the Yukawa matrices with the superscript d

$$Y_\nu^{(d)} = U_\nu^\dagger Y_\nu V_\nu, \quad Y_\ell^{(d)} = U_\ell^\dagger Y_\ell V_\ell, \quad (5)$$

and defines the PMNS matrix

$$U = U_\ell^\dagger U_\nu. \quad (6)$$

The relevant Lagrangian in the symmetric phase is then given by

$$Y_\nu^{(d)} \bar{\nu}_L (-\bar{\phi}^0) \nu_R + Y_\ell^{(d)} \bar{\ell}_L \phi^0 \ell_R + Y_\nu^{(d)} \bar{\ell}_L' \phi^- \nu_R + Y_\ell^{(d)} \bar{\nu}_L' \phi^+ \ell_R + h.c., \quad (7)$$

after the fermion field transformation, where the real component of ϕ^0 in the first two terms corresponds to the SM Higgs boson. The imaginary component of ϕ^0 and the charged scalars ϕ^\pm in the last two terms disappear after the symmetry breaking, and turn into the longitudinal components of weak gauge bosons. Equation (7) indicates that the Yukawa matrices have been diagonalized, but the charged scalar currents persist in the symmetric phase. Note that the left-handed charged leptons ℓ_L' , which couple to the right-handed neutrinos ν_R via charged scalar currents, differ from the physical mass eigenstates ℓ_L . The same differentiation applies to ν_L' and ν_L . The relations between them are governed by the PMNS matrix in Eq. (6),

$$\ell_L = U \ell_L', \quad \nu_L = U^\dagger \nu_L'; \quad (8)$$

namely, the left-hand sides are the linear combinations of the right-hand sides weighted by the PMNS matrix elements.

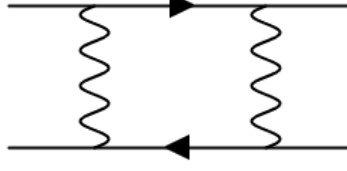


FIG. 1: Box diagram with the two vertical wavy lines representing W bosons.

The external neutral states $\mathcal{L}_L^- \ell_L^+$ and $\mathcal{L}_L^+ \ell_L^-$ are formed by the charged leptons in the broken phase, so their first emissions are composed of real neutral scalars or weak gauge bosons. As the magnitude of the \mathcal{L} invariant mass exceeds the restoration scale, internal leptons become massless, and start to exchange imaginary neutral scalars and charged scalars. The $\mathcal{L}_L^- \ell_L^+ - \mathcal{L}_L^+ \ell_L^-$ mixing must involve exchanges of charged scalars ϕ^\pm or W^\pm bosons in the symmetric phase. The Yukawa matrices associated with charged scalar emissions are also diagonal with $Y_\ell^{(d)}$ for the $\ell_R \rightarrow \nu'_L$ transition and $Y_\nu^{(d)}$ for the $\nu_R \rightarrow \ell'_L$ transition. When a right-handed neutrino ν_R emits a charged scalar ϕ^+ and transits to a left-handed charged lepton ℓ_L , which is one of the components of ℓ'_L according to Eq. (8), the emission is characterized by a PMNS matrix element. The same PMNS matrix element is associated with the W^+ boson mission in the $\nu_L \rightarrow \ell_L$ transition. This coincidence is expected, since a charged scalar is equivalent to the longitudinal component of a W boson.

The dispersion relation for the mixing amplitude $\Pi(s) \equiv M(s) - i\Gamma(s)/2$ is quoted as [21, 22]

$$M(s) = \frac{1}{2\pi} \int^R ds' \frac{\Gamma(s')}{s - s'} + \frac{1}{2\pi i} \int_{C_R} ds' \frac{\Pi(s')}{s' - s}, \quad (9)$$

where s is the mass squared of the heavy charged lepton \mathcal{L} , and $M(s)$ and $\Gamma(s)/2$ represent the real and imaginary parts of the mixing amplitude, respectively. The contour consists of one horizontal path below the branch cut along the positive real axis, another horizontal path above the branch cut, and a circle C_R of large radius R . The invariant mass squared s is located in a deep Euclidean region inside the large circle, far away from the branch cut, and its magnitude is above the restoration scale Λ^2 . We decompose the mixing amplitude into a sum over various intermediate neutrino channels,

$$\Pi(s) = \sum_{i,j=1}^3 \lambda_i \lambda_j \Pi_{ij}(s) + \cdots \equiv \sum_{i,j=1}^3 \lambda_i \lambda_j \left[M_{ij}(s) - \frac{i}{2} \Gamma_{ij}(s) \right] + \cdots, \quad (10)$$

where $\lambda_i \equiv U_{\mathcal{L}i}^* V_{\ell i}$ is the product of the PMNS matrix elements, and \cdots denote the contributions proportional to higher powers of $\lambda_{i,j}$. Because an intermediate state can be identified experimentally in principle, the contribution from each channel with the lowest power of $\lambda_i \lambda_j$ satisfies its own dispersion relation,

$$M_{ij}(s) = \frac{1}{2\pi} \int^R ds' \frac{\Gamma_{ij}(s')}{s - s'} + \frac{1}{2\pi i} \int_{C_R} ds' \frac{\Pi_{ij}(s')}{s' - s}, \quad (11)$$

in which the lower bound of s' for the dispersive integral of $\Gamma_{ij}(s')$ will be specified later.

A. Real Contribution

We calculate the real part of the mixing amplitude in the symmetric phase, and collect the detail in the Appendix. As elucidated above, the external states $\mathcal{L}_L^- \ell_L^+$ and $\mathcal{L}_L^+ \ell_L^-$ exchange only two W bosons at one-loop level as depicted by the box diagram in Fig. 1. The real contribution from the box diagrams with the massless internal neutrinos ν_{iL} , ν_{jL} and two massless W bosons is written as

$$M_{ij}^{(1)}(s) = -\frac{1}{16\pi^2} \left(\frac{g}{2\sqrt{2}} \right)^4 \frac{4}{s}, \quad (12)$$

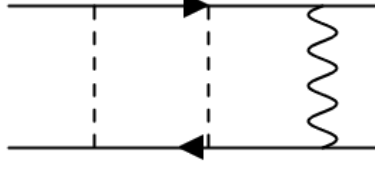


FIG. 2: Two-loop diagram with exchanges of a neutral scalar, a charged scalar and a W boson in sequence from left to right.

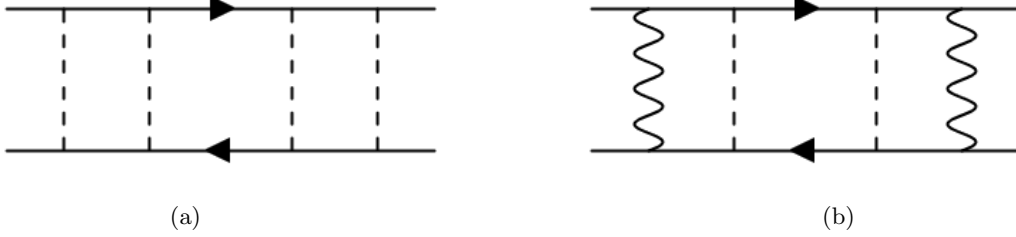


FIG. 3: (a) Three-loop diagram with exchanges of neutral, charged, charged and neutral scalars in sequence from left to right. (b) Three-loop diagram with exchanges of a W boson, two neutral scalars and a W boson in sequence from left to right.

which is of $O(g^4)$, g being the weak coupling. The above expression is independent of intermediate states, such that the summation over all intermediate channels vanishes owing to the unitarity condition $\sum_i U_{\mathcal{L}i}^* U_{\ell i} = 0$. The absence of the mixing dynamics in the symmetric phase has been adopted as the input in our previous LO analysis [1].

At two-loop level, the heavy charged lepton \mathcal{L}_L^- can first emit a Higgs boson, transiting to a right-handed charged lepton \mathcal{L}_R^- , which then emits a charged scalar ϕ^- , transiting to a left-handed neutrino ν_{iL} . At last, this ν_{iL} becomes the external charged lepton ℓ_L^- in the external state $\mathcal{L}_L^+ \ell_L^-$ by emitting a W^+ boson as illustrated in Fig. 2. All the above internal particles are massless. The Higgs boson vertex carries the Yukawa coupling, i.e., the diagonal element of the Yukawa matrix in Eq. (7), $(Y_\ell^{(d)})_{\mathcal{L}\mathcal{L}}/\sqrt{2} = m_{\mathcal{L}}/v$. The charged scalar vertex is characterized by the PMNS matrix element $U_{\mathcal{L}i}^*$ and the Yukawa coupling $(Y_\ell^{(d)})_{\mathcal{L}\mathcal{L}} = \sqrt{2}m_{\mathcal{L}}/v$ according to the Lagrangian in Eq. (7), and the W boson vertex contains the PMNS matrix element $U_{\ell i}$ and the weak coupling g . The combination of $U_{\mathcal{L}i}^*$ and $U_{\ell i}$ forms the PMNS factor λ_i . The couplings associated with the emissions from the external charged lepton ℓ_L^+ , the internal right-handed charged lepton \mathcal{L}_R^+ , and the internal left-handed neutrino ν_{jL} are assigned in a similar way, which gives rise to another PMNS factor λ_j . This contribution, unlike Eq. (12), is counted as $O(g^2)$ and the fourth power in the Yukawa couplings for charged leptons.

There are other two-loop diagrams of course. For instance, an additional photon or Z boson can be exchanged between the charged leptons in Fig. 1, or a W boson can proceed a hadronic decay, splitting into a quark-antiquark pair. These diagrams, being of higher orders in the electroweak coupling, are classified as radiative corrections to Fig. 1. To have them in the real part of the mixing amplitude, the corresponding diagrams must be added to the imaginary part for a consistent construction of the dispersion relation. We will not consider these contributions in the present order-of-magnitude investigation. The boson exchanges in the sequence of W^- , ϕ^+ and ϕ^0 , opposite to that displayed in Fig. 2, are allowed. The diagram involving a $\phi^0\phi^0\phi^+\phi^-$ four-scalar vertex and a W boson exchange also exists at $O(g^2)$. For our purpose, we compute only Fig. 2 in the Appendix, and the result reads

$$M_{ij}^{(2)}(s) = - \left(\frac{1}{16\pi^2} \right)^2 \left(\frac{g}{2\sqrt{2}} \right)^2 \frac{m_{\mathcal{L}}^2 m_\ell^2}{v^4} \frac{4}{s}. \quad (13)$$

The above formula, vanishing the summation over all intermediate channels, implies that the mixing phenomenon in the symmetric phase is still off at two-loop level. Note that the lepton mass dependence has been introduced via the Yukawa matrix $Y_\ell^{(d)}$, though all internal particles are massless in the symmetric phase.

We then extend the evaluation to three-loop level, at which there are even more diagrams. The contribution from exchanges of two W bosons and two charged scalars, being proportional to the PMNS factor to the fourth power, should be discarded. The diagram with exchanges of two photons (or two Z bosons) and two W bosons stands for

a higher-order correction in the electroweak coupling to Fig. 1, and is thus neglected. The contribution of Fig. 3(a) with two Higgs bosons and two charged scalars is proportional to $O(g^0)$ and the eighth power in the Yukawa couplings for charged leptons, different from Eqs. (12) and (13). At the same order, a Higgs boson can attach to \mathcal{L}_L^- and ℓ_L^- and another can attach to ℓ_L^+ and \mathcal{L}_L^+ ; the two Higgs bosons in the above diagram can cross each other; the external leptonic states can interact via two Higgs bosons and a $\phi^+\phi^+\phi^-\phi^-$ four-scalar vertex. Figure 3(b) with two W bosons and two neutral scalars [27], being proportional to (g^4) and the fourth power in the Yukawa couplings for neutrinos, also constitutes a higher-order correction to Fig. 1. Nevertheless, it produces the first piece of contributions dependent on intermediate neutrino masses, so that the summation over all intermediate channels does not vanish because of $\sum_i U_{\mathcal{L}i}^* U_{\ell i} (Y_\nu^{(d)})_{ii}^2 \neq 0$. Therefore, the reasoning for the disappearance of the mixing phenomenon in the symmetric phase [1] holds to an extremely high precision in view of the tininess of $Y_\nu^{(d)}$.

We estimate only the $O(g^0)$ contribution from Fig. 3(a) in the Appendix for our order-of-magnitude analysis, obtaining

$$M_{ij}^{(3)}(s) \approx \frac{1}{64} \left(\frac{1}{16\pi^2} \right)^3 \frac{m_{\mathcal{L}}^4 m_\ell^4}{v^8} \frac{3}{s}. \quad (14)$$

The contribution from Fig. 3(b) is also needed for discriminating the neutrino mass orderings in the next section, but its explicit expression is not crucial. We summarize the real part of the mixing amplitude in the symmetric phase from Eqs. (12), (13) and (14),

$$M_{ij}(s) \approx -\frac{1}{16\pi^2} \left[4 \left(\frac{g}{2\sqrt{2}} \right)^4 + \frac{1}{4\pi^2} \left(\frac{g}{2\sqrt{2}} \right)^2 \frac{m_{\mathcal{L}}^2 m_\ell^2}{v^4} - \frac{3}{64} \left(\frac{1}{16\pi^2} \right)^2 \frac{m_{\mathcal{L}}^4 m_\ell^4}{v^8} + O \left(g^4 \frac{m_i^2 m_j^2}{v^4} \right) \right] \frac{1}{s}, \quad (15)$$

where the last term is associated with Fig. 3(b). Equation (15) will be inserted into the left-hand side of the dispersion relation in Eq. (11).

B. Imaginary Contribution

The neutral leptonic states $\mathcal{L}_L^- \ell_L^+$ and $\mathcal{L}_L^+ \ell_L^-$ mix through the box diagrams with two W boson exchanges in the broken phase. To coordinate with the derivation of the real part $M_{ij}(s)$ in the previous subsection, we sum up the contributions to the imaginary part $\Gamma_{ij}(s)$ from all possible cuts on the internal lines in the box diagrams. This treatment differs from that in our earlier work [1], where only the two internal neutrino lines were cut. It makes sense, since such an intermediate state can be identified experimentally in principle, and the corresponding real part vanishes at LO owing to the unitarity of the PMNS matrix. The box diagrams induce the $(V-A)(V-A)$ and $(S-P)(S-P)$ structures, which ought to be handled separately. We concentrate on the former, which contributes [23, 24]

$$\begin{aligned} \Gamma_{ij}(s) &= \frac{G_F^2}{16\pi} \sum_k' \Gamma_{ij}^k(s), \\ \Gamma_{ij}^k(s) &= \int_{\alpha_k^l}^{\alpha_k^u} d\alpha \frac{(4m_W^4 + m_i^2 m_j^2) F_k(\alpha) - 4m_i^2 m_j^2 m_W^2 + 2s [\alpha m_i^2 + (1-\alpha)m_j^2] m_W^2}{(m_W^2 - m_i^2)(m_W^2 - m_j^2)}, \end{aligned} \quad (16)$$

with the notation $\sum_k' \equiv \sum_{k=1}^2 - \sum_{k=3}^4$ and the intermediate neutrino masses m_i and m_j .

The functions F_k take the forms

$$\begin{aligned} F_1(\alpha) &= \alpha m_i^2 + (1-\alpha)m_j^2 - \alpha(1-\alpha)s, \\ F_2(\alpha) &= m_W^2 - \alpha(1-\alpha)s, \\ F_3(\alpha) &= \alpha m_W^2 + (1-\alpha)m_j^2 - \alpha(1-\alpha)s, \\ F_4(\alpha) &= \alpha m_i^2 + (1-\alpha)m_W^2 - \alpha(1-\alpha)s, \end{aligned} \quad (17)$$

whose vanishing fixes the upper and lower bounds of the integration variable α ,

$$\begin{aligned}\alpha_1^{u,l} &= \frac{1}{2s} \left[s - m_i^2 + m_j^2 \pm \sqrt{s^2 - 2s(m_i^2 + m_j^2) + (m_i^2 - m_j^2)^2} \right], \\ \alpha_2^{u,l} &= \frac{1}{2s} \left[s \pm \sqrt{s^2 - 4sm_W^2} \right], \\ \alpha_3^{u,l} &= \frac{1}{2s} \left[s - m_W^2 + m_j^2 \pm \sqrt{s^2 - 2s(m_W^2 + m_j^2) + (m_W^2 - m_j^2)^2} \right], \\ \alpha_4^{u,l} &= \frac{1}{2s} \left[s - m_i^2 + m_W^2 \pm \sqrt{s^2 - 2s(m_i^2 + m_W^2) + (m_i^2 - m_W^2)^2} \right].\end{aligned}\quad (18)$$

The indices $k = 1, 2, 3$ and 4 correspond to the intermediate states with two real neutrinos, two real W bosons, the real neutrino of mass m_i and one real W boson, and the real neutrino of mass m_j and one real W boson, respectively. The thresholds for the dispersive integral in Eq. (11) are then set to the values $t_k = (m_i + m_j)^2$, $4m_W^2$, $(m_i + m_W)^2$ and $(m_j + m_W)^2$, respectively.

It is observed that the linear growth of $\Gamma_{ij}(s)$ at large s [1] in the broken phase cancels among the cuts in Eq. (16). The cancellation is so strong, that $\Gamma_{ij}(s)$ turns out to decrease like $1/s$ asymptotically. It is not hard to realize this strong cancellation; the functions F_k in Eq. (17), as well as the upper and lower bounds of α in Eq. (18), become identical in the $s \rightarrow \infty$ limit. The real part $M_{ij}(s)$ in Eq. (15) and the aforementioned decrease of $\Gamma_{ij}(s)$ at high s manifest that the mixing amplitude $\Pi_{ij}(s)$ goes down like $1/s$. Hence, the contour integral from the big circle diminishes with the radius R , and the large s' region does not contribute to the dispersive integral in Eq. (11). This fact is also reflected by the R independence of $M_{ij}(s)$ on the left-hand side of Eq. (11). Although the behavior of $\Gamma_{ij}(s)$ in the transition region between the symmetry broken and restored phases is unknown, physical insights can be extracted from the convergent dispersive integral. First, we remove the interval above the restoration scale, $\Lambda^2 < s' < R$, motivated by the disappearance of the R dependence. The restoration scale, representing an order-of-magnitude concept, can mimic the uncertainty associated with the transition region. The integration is then performed with the known integrand $\Gamma_{ij}(s')$ in Eq. (16), which is valid within the interval $t_k < s' < \Lambda^2$.

Keeping only the terms that survive in the large Λ^2 limit, we expand the dispersive integral as

$$\frac{1}{2\pi} \sum_k \int_{t_k}^{\Lambda^2} ds' \frac{\Gamma_{ij}^k(s')}{s - s'} \approx -\frac{G_F^2 m_W^4}{16\pi^2} \left[1 + \frac{m_i m_j}{m_W^2} \ln \frac{\Lambda^2}{m_W^2} - \frac{m_i^2 m_j^2}{m_W^4} \left(\ln \frac{m_W^2}{m_i m_j} - \frac{1}{4} \right) \right] \frac{2}{s}, \quad (19)$$

where the approximation $1/(s - s') \approx 1/s$ for $s \gg \Lambda^2$ has been applied, and those suppressed by higher powers of $m_{i,j}/m_W$ have been dropped for clarity. To proceed further, we recast the above expression, by employing the relations $G_F = \sqrt{2}g^2/(8m_W^2)$ and $m_W = gv/2$, into

$$\frac{1}{2\pi} \sum_k \int_{t_k}^{\Lambda^2} ds' \frac{\Gamma_{ij}(s')}{s - s'} \approx -\frac{1}{16\pi^2} \left[4 \left(\frac{g}{2\sqrt{2}} \right)^4 + 2 \left(\frac{g}{2\sqrt{2}} \right)^2 \frac{m_i m_j}{v^2} \ln \frac{\Lambda^2}{m_W^2} - \frac{m_i^2 m_j^2}{v^4} \left(\ln \frac{m_W^2}{m_i m_j} - \frac{1}{4} \right) \right] \frac{1}{s}. \quad (20)$$

It is noticed that powers of m_W have compensated some of the weak coupling, and the expansions on both sides of Eq. (11), i.e., in Eqs. (15) and (20), coincide perfectly in powers of g . In particular, the uncertainty from the transition region shows up only in the $O(g^2)$ term. Adding more photons, Z bosons and Higgs bosons to the box diagrams just introduces higher-order corrections to Eq. (20), which will be ignored in the present order-of-magnitude setup, as stated in the previous subsection.

III. SOLUTION

We are ready to acquire information on neutrino masses from Eq. (11), given the real piece $M_{ij}(s)$ in the symmetric phase and the imaginary piece $\Gamma_{ij}(s)$ in the broken phase. Our framework is appropriate for the mixing of heavy-light systems, like μe and τe . This claim is justified by the connections among the PMNS matrix elements discovered in our previous work [1]; the ratio $U_{\mu 1}^* U_{e 1}/(U_{\mu 2}^* U_{e 2})$ of the PMNS matrix elements for the μe mixing and $U_{\tau 1}^* U_{e 1}/(U_{\tau 2}^* U_{e 2})$ for the τe mixing are roughly equal, except the opposite signs of their imaginary parts. Such a prediction for heavy-light systems agrees well with the outcomes of global fits [7]. However, the ratio $U_{\tau 1}^* U_{\mu 1}/(U_{\tau 2}^* U_{\mu 2})$ for the $\tau \mu$ mixing does not follow the same pattern, suggesting that $\tau \mu$ should not be regarded as a heavy-light system. The distinction is natural in view of the charged lepton masses; a muon is about 200 times heavier than an electron, while a τ lepton is only 17 times heavier than a muon.

We have shown in Sec. IIA that $M_{ij}(s)$ in the symmetric phase is proportional to the masses of the external charged leptons. To probe how small a typical neutrino mass can be, we consider the μe mixing, and set $m_{i,j}$ in Eq. (20) to a common mass scale m_ν . As seen shortly, the value of m_ν determined from the dispersion relation is of order eV, so that there is no need to differentiate which generation of neutrinos this typical scale is assigned to; an eV scale is much higher than the measured mass differences reflected by $\Delta m_{21}^2 \equiv m_2^2 - m_1^2 = (7.55^{+0.20}_{-0.16}) \times 10^{-5} \text{ eV}^2$ and $\Delta m_{32}^2 \equiv m_3^2 - m_2^2 = (2.424 \pm 0.03) \times 10^{-3} \text{ eV}^2$ from the global fit [25]. We establish a solution to the dispersion relation by equating the terms in Eqs. (15) and (20) with the same powers of the weak coupling g , for g can vary freely in a mathematical viewpoint. It is immediately found that the first, i.e., $O(g^4)$, terms in Eqs. (15) and (20) are the same. We emphasize that this equality is insensitive to the behavior of $\Gamma_{ij}(s)$ in the transition region, namely, independent of the symmetry restoration scale.

The equality of the third, i.e., $O(g^0)$, terms in Eqs. (15) and (20) leads to Eq. (1), where $m_{\mathcal{L}}$, m_ℓ and $m_{i,j}$ have been replaced by the muon mass m_μ , the electron mass m_e , and the typical neutrino mass m_ν , respectively. The constant $1/4$ is negligible relative to the logarithmic term $\ln(m_W^2/m_\nu^2)$. Equation (1), arising from the convergent part of the dispersive integral, does not depend on the restoration scale either. It then designates a small mass scale for neutrinos unambiguously,

$$m_\nu \approx 3 \text{ eV}, \quad (21)$$

with the inputs $m_W \approx 80 \text{ GeV}$, $m_\mu \approx 0.1 \text{ GeV}$, $m_e \approx 0.5 \text{ MeV}$ and $v \approx 250 \text{ GeV}$ [7]. Note that this low mass scale $m_\nu \sim O(1) \text{ eV}$ is demanded by the internal consistency the SM dynamics, whose origin is quite different from the seesaw mechanism [18] as stated in the Introduction. Our order-of-magnitude estimate is not far beyond the upper bound on the neutrino mass $m_\nu < 0.9 \text{ eV}$ at 90% CL measured by the KATRIN Collaboration [19]. We mention that their measurement is independent of cosmological models and does not rely on assumptions whether a neutrino is a Dirac or Majorana particle.

Next we equate the second, i.e., $O(g^2)$, terms in Eqs. (15) and (20), reaching

$$m_\nu^2 \ln \frac{\Lambda}{m_W} \approx \frac{1}{16\pi^2} \frac{m_\mu^2 m_e^2}{v^2}, \quad (22)$$

whose combination with Eq. (1) yields Eq. (2). It is stressed that Eq. (2) is independent of the masses $m_{\mathcal{L}}$ and m_ℓ of the external charged leptons. Because of the uncertain behavior of $\Gamma_{ij}(s)$ in the transition region, we have regarded the coefficient on the right-hand side of Eq. (2) as being of $O(1)$. Unfortunately, the value of the restoration scale Λ inferred from Eq. (2) is sensitive to the $O(1)$ coefficient, so no definite result can be obtained (for a very crude guesstimate, Eq. (21) corresponds to $\Lambda \gtrsim O(100) \text{ TeV}$ via Eq. (2)). Instead, we highlight the essential indication that the large electroweak symmetry restoration, i.e., new physics scale is tied to the tiny neutrino mass. A precise prediction for the new physics scale can be achieved by exploring $\Gamma_{ij}(s)$ in the transition region and by calculating exact multi-loop contributions to $M_{ij}(s)$ in the symmetric phase.

At last, we sum both Eq. (15) and (20) over all intermediate channels, and check whether the constraint on the PMNS matrix elements and the neutrino mass orderings in our previous LO analysis [1] is maintained. Only the $O(m_i^2 m_j^2 / v^4)$ term in Eq. (15), which depends on the intermediate neutrino masses, survives the summation under the unitarity of the PMNS matrix. The summation for Eq. (20) is dominated by the second term of $O(m_i m_j / v^2)$. The elimination of $\lambda_3 = -\lambda_1 - \lambda_2$ by means of the unitarity condition produces

$$\ln \frac{\Lambda^2}{m_W^2} [\lambda_1(m_3 - m_1) + \lambda_2(m_3 - m_2)]^2 = \sum_{i,j} O\left(\frac{m_i^2 m_j^2}{v^2}\right) \approx 0, \quad (23)$$

which leads to Eq. (3) trivially irrespective of the restoration scale Λ ; the $O(m_i m_j)$ coefficient of $\ln(\Lambda^2/m_W^2)$ must diminish to match the right-hand side of $O(m_i^2 m_j^2 / v^2)$.

To facilitate the discussion, we quote the PMNS matrix in the Chau-Keung parametrization [26],

$$U_{\text{PMNS}} = \begin{pmatrix} c_{12}c_{13} & s_{12}c_{13} & s_{13}e^{-i\delta} \\ -s_{12}c_{23} - c_{12}s_{23}s_{13}e^{i\delta} & c_{12}c_{23} - s_{12}s_{23}s_{13}e^{i\delta} & s_{23}c_{13} \\ s_{12}s_{23} - c_{12}c_{23}s_{13}e^{i\delta} & -c_{12}s_{23} - s_{12}c_{23}s_{13}e^{i\delta} & c_{23}c_{13} \end{pmatrix}, \quad (24)$$

with the notations $s_{12} \equiv \sin \theta_{12}$, $c_{12} \equiv \cos \theta_{12}$, etc. for the mixing angles, and the CP phase δ . The products of the PMNS matrix elements then read

$$\lambda_1 = -c_{12}c_{13} (s_{12}c_{23} + c_{12}s_{23}s_{13}e^{-i\delta}), \quad \lambda_2 = s_{12}c_{13} (c_{12}c_{23} - s_{12}s_{23}s_{13}e^{-i\delta}). \quad (25)$$

Defining $r = \lambda_1/\lambda_2$, we require the cancellation between the real parts of $r(m_3 - m_1)$ and $(m_3 - m_2)$ according to Eq. (3),

$$\text{Rer}(m_3 - m_1) + (m_3 - m_2) \approx 0, \quad (26)$$

and the small imaginary part of $r(m_3 - m_1)$, i.e., a small $s_\delta \equiv \sin \delta$.

It is easy to verify that the mixing angles $\theta_{12} = (34.5^{+1.2}_{-1.0})^\circ$, $\theta_{13} = (8.45^{+0.16}_{-0.14})^\circ$ and $\theta_{23} = (47.7^{+1.2}_{-1.7})^\circ$, and the CP phase $\delta = (218^{+38}_{-27})^\circ$ from the global fit [25] in the NO scenario meet better the above requirements, compared to $\theta_{12} = (34.5^{+1.2}_{-1.0})^\circ$, $\theta_{13} = (8.53^{+0.14}_{-0.15})^\circ$, $\theta_{23} = (47.9^{+1.0}_{-1.7})^\circ$ and $\delta = (281^{+23}_{-27})^\circ$ in the IO one [25]. We set θ_{12} , θ_{13} and θ_{23} to their central values owing to their small errors, and vary δ within its 1- σ range. Equation (26) can be satisfied by $c_\delta < 0$ ($\text{Rer} > -1$) and $m_3 - m_1 > 0$ for the NO, and by $c_\delta > 0$ ($\text{Rer} < -1$) and $m_3 - m_1 < 0$ for the IO. The whole range of δ for the NO is allowed, for the resultant Rer takes values between -0.9 and -0.7 , while δ in the IO case is restricted to $(270^\circ, 304^\circ)$. We then have $s_\delta \approx -(0.62^{+0.35}_{-0.43})$ from the NO, whose magnitude could be much lower than that of $s_\delta \in (-1, -0.83)$ from the IO. The latter narrow range is attributed to that δ for the IO is about $3\pi/2$, so the amount of errors similar to the NO case causes minor variation of s_δ . Our solution favors negative c_δ and diminishing s_δ , i.e., $\delta \sim 180^\circ$, close to that derived in a seesaw model with right-handed neutrino masses being dynamically generated by strong horizontal gauge interactions [13].

IV. CONCLUSION

We have proposed a viable explanation on the extremely small neutrino masses, which comes as a straightforward extension of our continuous efforts in understanding the SM flavor structure. Dispersion relations, which analytical physical observables must obey, bind interactions at various scales, and enforce stringent constraints on the SM parameters. The assumption for the existence of an electroweak symmetric phase grants such a bond between the dynamics above and below the symmetry restoration scale. We have taken into account the contributions to the mixing of neutral leptonic states up to three loops in the symmetric phase, which arise from the exchanges of neutral and charged scalars and W bosons. The standard box diagrams responsible for the mixing in the symmetry broken phase involve the neutrino masses and the PMNS matrix elements. It was then demonstrated that the dispersion relation for the $\mu^- e^+ - \mu^+ e^-$ mixing demands a typical neutrino mass scale m_ν at eV order in the SM unambiguously. It is much lower than a lepton mass because of the huge suppression factor m_ℓ/v formed by the lepton mass and the electroweak scale. At two-loop level, the dispersion relation hints that the large electroweak symmetry restoration, i.e., new physics scale is linked to the small neutrino mass.

The calculation presented in the Appendix confirmed that the disappearance of the mixing phenomenon in the symmetric phase, argued in our previous publication based on the unitarity of the PMNS matrix, holds to high precision, up to corrections of $O(m_\nu^4/v^4)$. In other words, the first nonvanishing contribution which survives the summation over all intermediate channels stars at three-loop level. It is thus expected that the dispersive constraint on the neutrino masses and the PMNS matrix elements with the loop corrections still prefers the NO over the IO. The pivot for discriminating the neutrino mass orderings is played by the CP phase, which got distinct results in the global fits for the NO and the IO. Since it is challenging to determine the neutrino mass spectrum experimentally, our theoretical attempt should be worthwhile. The above summarizes the solution to the dispersion relation for the mixing of heavy-light leptonic systems. We admit that our approach is preliminary, accurate only to orders of magnitude, and needs to be refined in the future. In principle, more definite predictions for the neutrino masses and for the new physics scale can be made by exploring the imaginary piece $\Gamma_{ij}(s)$ in the transition region and by computing complete multi-loop contributions to the real piece $M_{ij}(s)$ in the symmetric phase.

We affirm that the current formalism for generating a small neutrino mass cannot be extended to the quark case, simply due to strong interaction among quarks. The strong coupling $g_s \gtrsim 1$ is much larger than most of the quark Yukawa couplings, even greater than the top Yukawa coupling, such that the loop corrections discussed in this work are overwhelmed by QCD ones. For example, the two neutral scalars in Fig. 3(a) for the mixing between the neutral quark states $\bar{c}u$ and $\bar{u}c$ can be replaced by two gluons. The resultant contribution then dominates over the former one by a factor $g_s^4 v^4/(m_c^2 m_u^2) \gg 1$ with the charm (up) quark mass m_c (m_u). It is obvious that Eq. (1) is not justified. In this sense, the origin of the tiny neutrino mass traces back to the fact that a neutrino participates only weak and scalar interactions. Combining the present and previous observations, we conjecture that the mass hierarchy inherent in the SM, from the neutrino masses up to the electroweak scale, and the distinct quark and lepton mixing patterns, may be accommodated by means of the internal consistency of the SM dynamics. This understanding also points to possible new physics scenarios above the electroweak symmetry restoration scale, such as the composite Higgs model, which will be explored in forthcoming papers.

Acknowledgement

We thank Y. Chung, X.G. He, Y.B. Hsiung, Y. Liao, J.L. Liu and M.R. Wu for illuminating discussions. This work was supported in part by National Science and Technology Council of the Republic of China under Grant No. MOST-110-2112-M-001-026-MY3.

Appendix A: MIXING AMPLITUDE UP TO THREE LOOPS IN SYMMETRIC PHASE

1. One Loop

The box-diagram contribution, including both the real and imaginary parts, has been computed in [24]. We set the intermediate neutrino masses to zero, and then take the $m_W \rightarrow 0$ limit to get the leading real contribution in the symmetric phase shown in Eq. (12). The dispersion relation at $O(g^4)$ is then verified by Eqs. (15) and (20). To reduce the load for two-loop and three-loop calculations, we propose a simplified scheme below. The amplitude from the box diagram in Fig. 1 for the $\mathcal{L}^-\ell^+-\mathcal{L}^+\ell^-$ mixing with massless intermediate particles is written as

$$-i\mathcal{M} = \frac{1}{2} \left(\frac{-ig}{2\sqrt{2}} \right)^4 \int \frac{d^4l}{(2\pi)^4} \frac{\bar{u}_\ell \gamma_\nu (1 - \gamma_5) i(\not{p} - \not{l}) \gamma_\mu (1 - \gamma_5) u_\mathcal{L} \bar{v}_\ell \gamma_{\mu'} (1 - \gamma_5) (-i) \not{l} \gamma_{\nu'} (1 - \gamma_5) v_\mathcal{L} (-i)^2 g^{\nu\nu'} g^{\mu\mu'}}{(l^2 + i\epsilon)^2 [(p - l)^2 + i\epsilon]^2}. \quad (\text{A1})$$

The PMNS matrix elements have been suppressed, the spin factor 1/2 comes from the definition of the neutral leptonic state, the coupling $-ig/(2\sqrt{2})$ is associated with a weak vertex, and the tensors $g^{\nu\nu'}$ and $g^{\mu\mu'}$ are from the massless W boson propagators. Strictly speaking, the aforementioned $m_W \rightarrow 0$ limit urges that we start with a massive m_W boson propagator,

$$-i \frac{g^{\mu\mu'} - l^\mu l^{\mu'} / m_W^2}{l^2 - m_W^2}, \quad (\text{A2})$$

involving an additional longitudinal polarization. Here we employ a massless W boson propagator directly for simplification.

The Fierz identity is inserted into Eq. (A1) to factorize the lepton currents,

$$\mathcal{M} = -\frac{1}{4} \left(\frac{g}{2\sqrt{2}} \right)^4 \bar{u}_\ell \gamma^\alpha (1 - \gamma_5) u_\mathcal{L} \bar{v}_\ell \gamma^\beta (1 - \gamma_5) v_\mathcal{L} i \int \frac{d^4l}{(2\pi)^4} \frac{\text{tr}[\gamma_\mu \gamma_\alpha \gamma^\mu \not{l} \gamma_\nu \gamma_\beta \gamma_\nu (\not{p} - \not{l})(1 + \gamma_5)]}{(l^2 + i\epsilon)^2 [(p - l)^2 + i\epsilon]^2}. \quad (\text{A3})$$

If we work on the $(S - P)(S - P)$ structure, the term $(1 - \gamma_5) \otimes (1 - \gamma_5)$ in the Fierz identity will need to be inserted too, and the derivation will be more cumbersome. To extract the $(V - A)(V - A)$ current, we delete the current product $\bar{u}_\ell \gamma^\alpha (1 - \gamma_5) u_\mathcal{L} \bar{v}_\ell \gamma^\beta (1 - \gamma_5) v_\mathcal{L}$, and contract the remaining piece by the projector $g^{\alpha\beta}/4$. The projector should be $(g^{\alpha\beta} - p^\alpha p^\beta / p^2)/3$ to avoid the $(S - P)(S - P)$ component. However, we have confirmed that $g^{\alpha\beta}/4$ reproduces Eq. (12) from Eq. (A1) with massless W boson propagators. This simpler scheme will be applied to the evaluations of two-loop and three-loop diagrams for an order-of-magnitude estimate. We acquire from Fig. 1

$$\mathcal{M} = 2 \left(\frac{g}{2\sqrt{2}} \right)^4 i \int \frac{d^4l}{(2\pi)^4} \frac{l \cdot (p - l)}{(l^2 + i\epsilon)^2 [(p - l)^2 + i\epsilon]^2} = \frac{2}{16\pi^2} \left(\frac{g}{2\sqrt{2}} \right)^4 \frac{1}{s}, \quad (\text{A4})$$

with $s = p^2$, which is assumed to be in the Euclidean region.

We have quoted the imaginary contribution of the box diagrams in the broken phase from [24] as stated in Sec. II. It is reminded that the analysis in [24] was conducted for the mixing of neutral quark states. A quark possesses degrees of freedom from colors, and the box diagrams with vertical W boson lines (in Fig. 1) and with horizontal W boson lines have different color factors, 1 for the former and 3 for the latter. Since a color factor can vary arbitrarily in a mathematical viewpoint, each box diagram respects its own dispersion relation. We will take advantage of this fact for the leptonic state mixing, combining the above two box diagrams in the way the same as in the quark case, although a lepton has no color charge. The contribution from the second box diagram with horizontal W boson lines turns out to be identical to Eq. (A4) but with an opposite sign. The combination of the two box diagrams then yields Eq. (12). We do not include the diagram with the two W bosons in the second diagram crossing each other, because it obeys a separate dispersion relation with different branch cuts; the two intermediate neutrinos of unequal masses cannot be on shell simultaneously in this case.

2. Two Loops

The two-loop diagram in Fig. 2 contributes in the symmetric phase

$$-i\mathcal{M} = \frac{1}{2} \left(-i\frac{m_{\mathcal{L}}}{v}\right) \left(-i\frac{\sqrt{2}m_{\mathcal{L}}}{v}\right) \left(-i\frac{m_{\ell}}{v}\right) \left(-i\frac{\sqrt{2}m_{\ell}}{v}\right) \left(\frac{-ig}{2\sqrt{2}}\right)^2 \int \frac{d^4l_1}{(2\pi)^4} \int \frac{d^4l_2}{(2\pi)^4} \\ \times \frac{\bar{u}_{\ell}\gamma_{\mu}(1-\gamma_5)i(\not{p}-\not{l}_2)i(\not{p}-\not{l}_1)u_{\mathcal{L}}\bar{v}_{\ell}(-i)\not{l}_1(-i)\not{l}_2\gamma_{\nu}(1-\gamma_5)v_{\mathcal{L}}}{(p-l_2)^2(p-l_1)^2l_1^2l_2^2} \frac{i}{l_1^2} \frac{i}{(l_2-l_1)^2} \frac{-ig^{\mu\nu}}{(p-l_2)^2}, \quad (\text{A5})$$

where the Yukawa couplings for the neutral and charged scalar emissions have been specified in Sec. II. Inserting the Fierz identity to factorize the lepton currents and contracting the remaining part by the projector $g^{\alpha\beta}/4$, we have

$$\mathcal{M} = -\frac{m_{\mathcal{L}}^2 m_{\ell}^2}{v^4} \left(\frac{g}{2\sqrt{2}}\right)^2 \int \frac{d^4l_1}{(2\pi)^4} \int \frac{d^4l_2}{(2\pi)^4} \frac{l_1 \cdot l_2 (p-l_2) \cdot (p-l_1)}{((p-l_2)^2)^2 (p-l_1)^2 (l_1^2)^2 (l_2^2)^2 (l_2-l_1)^2}. \quad (\text{A6})$$

We first work out the integration over l_1 under the Feynman parametrization,

$$\int \frac{d^4l_1}{(2\pi)^4} \frac{l_1 \cdot l_2 (p-l_2) \cdot (p-l_1)}{(l_1^2)^2 (p-l_1)^2 (l_2-l_1)^2} = 6 \int_0^1 dv \int_0^{1-v} du (1-u-v) \int \frac{d^4l_1}{(2\pi)^4} \frac{l_1 \cdot l_2 (p-l_2) \cdot (p-l_1)}{[l_1^2 - 2up \cdot l_1 + us - 2vl_2 \cdot l_1 + vl_2^2]^4}. \quad (\text{A7})$$

The variable change $l_1 \rightarrow l_1 + up + vl_2$ and the Wick rotation lead the above integral to

$$\frac{i\pi^2}{(2\pi)^4} \int_0^1 dv \int_0^{1-v} du (1-u-v) \left\{ \frac{(up + vl_2) \cdot l_2 (p-l_2) \cdot [(1-u)p - vl_2]}{[v(1-v)l_2^2 - 2uwp \cdot l_2 + u(1-u)s]^2} \right. \\ \left. - \frac{(p-l_2) \cdot l_2}{2[v(1-v)l_2^2 - 2uwp \cdot l_2 + u(1-u)s]} \right\}. \quad (\text{A8})$$

We then turn to the integration over l_2 . The first piece in Eq. (A8) gives, under the Feynman parametrization,

$$I_1 = \int \frac{d^4l_2}{(2\pi)^4} \frac{(up + vl_2) \cdot l_2 (p-l_2) \cdot [(1-u)p - vl_2]}{l_2^2 ((p-l_2)^2)^2 [v(1-v)l_2^2 - 2uwp \cdot l_2 + u(1-u)s]^2} \\ = \int_0^1 dw \int_0^{1-w} dt \frac{24tw}{v^2(1-v)^2} \int \frac{d^4l_2}{(2\pi)^4} \frac{(up + vl_2) \cdot l_2 (p-l_2) \cdot [(1-u)p - vl_2]}{\{l_2^2 - 2tp \cdot l_2 - 2uwp \cdot l_2/(1-v) + ts + u(1-u)ws/[v(1-v)]\}^5}. \quad (\text{A9})$$

The variable change

$$l_2 \rightarrow l_2 + \left(t + \frac{uw}{1-v}\right)p \quad (\text{A10})$$

brings Eq. (A9) into

$$I_1 = \frac{i\pi^2}{(2\pi)^4} \int_0^1 dw \int_0^{1-w} dt \frac{2tw}{(1-v)^2} \frac{A(B+D) + (B-C)D + 3D^2}{D^3}, \quad (\text{A11})$$

with the functions

$$A = \left(\frac{u}{v} + t + \frac{uw}{1-v}\right) \left(t + \frac{uw}{1-v}\right) s \\ B = \left(1 - t - \frac{uw}{1-v}\right) \left(\frac{1-u}{v} - t - \frac{uw}{1-v}\right) s \\ C = \left(\frac{u}{v} + 2t + \frac{2uw}{1-v}\right) \left(1 + \frac{1-u}{v} - 2t - \frac{2uw}{1-v}\right) \frac{s}{4} \\ D = \left[t + \frac{u(1-u)w}{v(1-v)}\right] s - \left(t + \frac{uw}{1-v}\right)^2 s. \quad (\text{A12})$$

We calculate the second term in Eq. (A8) in a similar way,

$$I_2 = \frac{1}{2} \int \frac{d^4l_2}{(2\pi)^4} \frac{(l_2-p) \cdot l_2}{l_2^2 ((p-l_2)^2)^2 [v(1-v)l_2^2 - 2uwp \cdot l_2 + u(1-u)s]} \\ = \int_0^1 dw \int_0^{1-w} dt \frac{6t}{2v(1-v)} \int \frac{d^4l_2}{(2\pi)^4} \frac{(l_2-p) \cdot l_2}{\{l_2^2 - 2tp \cdot l_2 - 2uwp \cdot l_2/(1-v) + ts + u(1-u)ws/[v(1-v)]\}^4}. \quad (\text{A13})$$

The same variable change in Eq. (A10) generates

$$I_2 = \frac{i\pi^2}{(2\pi)^4} \int_0^1 dw \int_0^{1-w} dt \frac{t}{2v(1-v)} \frac{2D-E}{D^2}, \quad (\text{A14})$$

with the function

$$E = \left(1 - t - \frac{uw}{1-v}\right) \left(t + \frac{uw}{1-v}\right) s. \quad (\text{A15})$$

At last, the contribution from Fig. 2 reads

$$\begin{aligned} \mathcal{M} &= -\frac{m_{\mathcal{L}}^2 m_\ell^2}{v^4} \left(\frac{g}{2\sqrt{2}}\right)^2 \frac{i\pi^2}{(2\pi)^4} \int_0^1 dv \int_0^{1-v} du (1-u-v)(I_1 + I_2) \\ &= \frac{m_{\mathcal{L}}^2 m_\ell^2}{v^4} \left(\frac{g}{2\sqrt{2}}\right)^2 \left(\frac{1}{16\pi^2}\right)^2 \frac{2}{s}, \end{aligned} \quad (\text{A16})$$

where the integrations over the Feynman parameters u , v , t and w are carried out numerically. The result from the diagram with horizontal boson lines is has the same expression but with an opposite sign. Following the special combination of the two diagrams, we arrive at Eq. (13).

3. Three Loops

The three-loop diagram with four vertical scalar lines in Fig. 3(a) contains the loop integral

$$\begin{aligned} -i\mathcal{M} &= \frac{1}{2} \left(-i\frac{m_{\mathcal{L}}}{v}\right)^2 \left(-i\frac{\sqrt{2}m_{\mathcal{L}}}{v}\right)^2 \left(-i\frac{m_\ell}{v}\right)^2 \left(-i\frac{\sqrt{2}m_\ell}{v}\right)^2 \int \frac{d^4 l_1}{(2\pi)^4} \int \frac{d^4 l_2}{(2\pi)^4} \int \frac{d^4 l_3}{(2\pi)^4} \\ &\times \frac{\bar{u}_\ell i \not{l}_3 i \not{l}_2 i (\not{p} - \not{l}_1) u_{\mathcal{L}} \bar{v}_\ell (-i) \not{l}_1 (-i) (\not{p} - \not{l}_2) (-i) (\not{p} - \not{l}_3) v_{\mathcal{L}}}{(p-l_1)^2 (p-l_2)^2 (p-l_3)^2 l_1^2 l_2^2 l_3^2} \frac{i}{l_1^2} \frac{i}{(p-l_1-l_2)^2} \frac{i}{(l_2-l_3)^2} \frac{i}{l_3^2}. \end{aligned} \quad (\text{A17})$$

We have arranged the loop momentum flows to facilitate the identification of the leading regions for the integral. It is straightforward to tell that finite l_1 gives an important contribution, for both the infrared and ultraviolet regions are suppressed. Small l_2 dominates, in which the integration over l_3 develops an infrared logarithmic enhancement. We thus neglect l_2 in the factor $p-l_1-l_2$, such that the integration over l_1 is simplified to the one for the box diagram in Fig. 1, and retain only the terms up to those linear in l_2 in the integral over l_3 . An order-of-magnitude estimate serves our purpose, so the above approximation is appropriate, without which the handling of three-loop diagrams would be extremely tedious. The reasoning then motivates the separation of Eq. (A17) into three pieces by inserting the Fierz identity,

$$\begin{aligned} \mathcal{M} &= \frac{2i}{8^4} \frac{m_{\mathcal{L}}^4 m_\ell^4}{v^8} \bar{u}_\ell \gamma^\alpha (1-\gamma_5) u_{\mathcal{L}} \bar{v}_\ell \gamma^\beta (1-\gamma_5) v_{\mathcal{L}} \\ &\times \int \frac{d^4 l_2}{(2\pi)^4} \frac{\text{tr}[(\not{p} - \not{l}_2) \gamma^\lambda (1-\gamma_5) \not{l}_2 \gamma^\sigma (1-\gamma_5)]}{(p-l_2)^2 l_2^2} \\ &\times \int \frac{d^4 l_1}{(2\pi)^4} \frac{\text{tr}[\not{l}_1 (1-\gamma_5) \gamma_\sigma (\not{p} - \not{l}_1) (1-\gamma_5) \gamma_\alpha]}{(p-l_1)^2 (p-l_1-l_2)^2 (l_1^2)^2} \\ &\times \int \frac{d^4 l_3}{(2\pi)^4} \frac{\text{tr}[(\not{p} - \not{l}_3) (1-\gamma_5) \gamma_\beta \not{l}_3 (1-\gamma_5) \gamma_\lambda]}{(p-l_3)^2 (l_3^2)^2 (l_2-l_3)^2}. \end{aligned} \quad (\text{A18})$$

The integral over l_1 is denoted by

$$J_1 = \int \frac{d^4 l_1}{(2\pi)^4} \frac{\text{tr}[\not{l}_1 (1-\gamma_5) \gamma_\sigma (\not{p} - \not{l}_1) (1-\gamma_5) \gamma_\alpha]}{(p-l_1)^2 (p-l_1-l_2)^2 (l_1^2)^2} \approx 2 \int \frac{d^4 l_1}{(2\pi)^4} \frac{\text{tr}[\not{l}_1 \gamma_\sigma (\not{p} - \not{l}_1) \gamma_\alpha (1+\gamma_5)]}{((p-l_1)^2)^2 (l_1^2)^2}, \quad (\text{A19})$$

in the small l_2 region. The matrix γ_5 does not contribute, because the vectors p and l_1 must appear in even powers after the Feynman parametrization. Equation (A19) becomes

$$J_1 \approx 24 \int_0^1 du u(1-u) \int \frac{d^4 l_1}{(2\pi)^4} \frac{4u(1-u)p_\alpha p_\sigma - g_{\alpha\sigma}[l_1^2 + 2u(1-u)s]}{[l_1^2 - u(1-u)s]^4} = \frac{i}{\pi^2} \frac{p_\alpha p_\sigma}{s^2}, \quad (\text{A20})$$

where the portion proportional to $g_{\alpha\sigma}$ turns out to vanish.

The third integral is computed as

$$\begin{aligned}
J_3 &= \int \frac{d^4 l_3}{(2\pi)^4} \frac{\text{tr}[(\not{p} - \not{l}_3)(1 - \gamma_5)\gamma_\beta \not{l}_3(1 - \gamma_5)\gamma_\lambda]}{(p - l_3)^2 (l_3^2)^2 (l_2 - l_3)^2} \\
&= 12 \int_0^1 du \int_0^{1-u} dv (1 - u - v) i \int \frac{d^4 l_3}{(2\pi)^4} \\
&\quad \times \frac{2(up + vl_2)_\lambda [(1 - u)p - vl_2]_\beta + 2(up + vl_2)_\beta [(1 - u)p - vl_2]_\lambda - g_{\lambda\beta} \{l_3^2 + 2(up + vl_2) \cdot [(1 - u)p - vl_2]\}}{[l_3^2 - u(1 - u)s - v(1 - v)l_2^2 + 2uvp \cdot l_2]^4},
\end{aligned} \tag{A21}$$

to which the Feynman parametrization and the variable change $l_3 \rightarrow l_3 + up + vl_2$ have been implemented. Keeping the terms up to those linear in l_2 , we get

$$\begin{aligned}
J_3 &\approx \frac{i}{4\pi^2} \int_0^1 du \int_0^{1-u} dv (1 - u - v) \frac{2u(1 - u)p_\lambda p_\beta - (1 - 2u)vl_{2\lambda}p_\beta + (1 - 2u)vp_\lambda l_{2\beta} + g_{\lambda\beta}(1 - 2u)vp \cdot l_2}{[u(1 - u)s + v(1 - v)l_2^2 - 2uvp \cdot l_2]^2} \\
&\approx \frac{i}{4\pi^2} \left[\frac{2p_\lambda p_\beta}{s^2} \ln \frac{s}{l_2^2} + (g_{\lambda\beta}p \cdot l_2 - l_{2\lambda}p_\beta + p_\lambda l_{2\beta}) \frac{1}{sl_2^2} \right].
\end{aligned} \tag{A22}$$

To reach the last expression, we have focused on the leading region with small u and v , i.e., on the terms linear in u and v .

We then work out the integral over l_2 in the small l_2 region,

$$\begin{aligned}
J_2 &= \frac{i}{4\pi^2} \int \frac{d^4 l_2}{(2\pi)^4} \frac{\text{tr}[(\not{p} - \not{l}_2)\gamma^\lambda(1 - \gamma_5) \not{l}_2\gamma^\sigma(1 - \gamma_5)]}{(p - l_2)^2 l_2^2} \left[\frac{2p_\lambda p_\beta}{s^2} \ln \frac{s}{l_2^2} + (g_{\lambda\beta}p \cdot l_2 - l_{2\lambda}p_\beta + p_\lambda l_{2\beta}) \frac{1}{sl_2^2} \right] \\
&\approx \frac{2i}{\pi^2} \int \frac{d^4 l_2}{(2\pi)^4} \frac{p^\lambda l_2^\sigma + l_2^\lambda p^\sigma - g^{\lambda\sigma} l_2 \cdot p}{sl_2^2} \left[\frac{2p \cdot l_2}{s} \frac{2p_\lambda p_\beta}{s^2} \ln \frac{s}{l_2^2} + (g_{\lambda\beta}p \cdot l_2 - l_{2\lambda}p_\beta + p_\lambda l_{2\beta}) \frac{1}{sl_2^2} \right],
\end{aligned} \tag{A23}$$

where the expansion of the denominator $(p - l_2)^2 + i\epsilon \approx p^2 - 2p \cdot l_2 + i\epsilon$ in powers of l_2 has been made. The above integral reduces to

$$\begin{aligned}
J_2 &\approx \frac{2i}{\pi^2} \int \frac{d^4 l_2}{(2\pi)^4} \frac{1}{s^2} \left[\frac{4l_2^\sigma p \cdot l_2 p_\beta}{sl_2^2} \ln \frac{s}{l_2^2} + \frac{sl_2^\sigma l_{2\beta} - l_2^2 p^\sigma p_\beta + p \cdot l_2 p^\sigma l_{2\beta} + p \cdot l_2 l_2^\sigma p_\beta - g_\beta^\sigma (p \cdot l_2)^2}{(l_2^2)^2} \right] \\
&\approx \frac{3}{64\pi^4} \frac{p^\sigma p_\beta}{s}.
\end{aligned} \tag{A24}$$

Note that the Wick rotation of the zeroth component of l_2 introduces $-i$, instead of $+i$, since the pole is located in the first quadrant as indicated by the denominator $p^2 - 2p \cdot l_2 + i\epsilon$ in Eq. (A23). We have restricted the range of the integration variable to $0 < l_2^2 < s/2$ after the Wick rotation in accordance with the soft approximation.

At last, we group all the ingredients together, remove the lepton currents, and contract the remaining part by $g^{\alpha\beta}/4$, deriving

$$\mathcal{M} \approx \frac{2i}{8^4} \frac{m_{\mathcal{L}}^4 m_\ell^4}{v^8} \frac{g^{\alpha\beta}}{4} \frac{i}{\pi^2} \frac{p_\alpha p_\sigma}{s^2} \frac{3}{64\pi^4} \frac{p^\sigma p_\beta}{s} = -\frac{3}{128} \left(\frac{1}{16\pi^2} \right)^3 \frac{m_{\mathcal{L}}^4 m_\ell^4}{v^8} \frac{1}{s}. \tag{A25}$$

The combination with the contribution from the diagram with horizontal scalar lines then produces Eq. (14).

-
- [1] H. n. Li, [arXiv:2306.03463 [hep-ph]].
 - [2] H. n. Li, Phys. Rev. D **107**, 094007 (2023).
 - [3] H. n. Li, Phys. Rev. D **108**, no.5, 054020 (2023).
 - [4] Y. T. Chien and H. n. Li, Phys. Rev. D **97**, 053006 (2018).
 - [5] L. Huang, S. D. Lane, I. M. Lewis and Z. Liu, Phys. Rev. D **103**, 053007 (2021).
 - [6] D. B. Kaplan and H. Georgi, Phys. Lett. B **136**, 183 (1984).
 - [7] R.L. Workman et al. (Particle Data Group), Prog. Theor. Exp. Phys. 2022, 083C01 (2022).
 - [8] J. S. Alvarado and R. Martinez, [arXiv:2007.14519 [hep-ph]].
 - [9] G. Xu and Y. Zhang, EPL **143**, 44001 (2023).

- [10] A. A. Patel and T. P. Singh, Universe **9**, 440 (2023).
- [11] H. Bora, N. K. Francis, A. Barman and B. Thapa, Phys. Lett. B **848**, 138329 (2024).
- [12] B. Thapa, S. Barman, S. Bora and N. K. Francis, JHEP **11**, 154 (2023).
- [13] Y. Chung, [arXiv:2311.17183 [hep-ph]].
- [14] S. Supanyo, C. Hasuwannakit, S. Yoo-Kong, L. Tannukij and M. Tanasittikosol, [arXiv:2312.16587 [hep-ph]].
- [15] B. Lampe, PoS **EPS-HEP2023**, 373 (2024).
- [16] A. R. Shaikh and R. Adhikari, [arXiv:2404.11570 [hep-ph]].
- [17] S. M. Bilenky, C. Giunti, J. A. Grifols and E. Masso, Phys. Rept. **379**, 69 (2003).
- [18] P. Minkowski, Phys. Lett. **67B**, 421 (1977); M. Gell-Mann, P. Ramond, and R. Slansky, Conf. Proc. C790927, 315 (1979); T. Yanagida, Conf. Proc. C7902131, 95 (1979); R. N. Mohapatra and G. Senjanovic, Phys. Rev. Lett. **44**, 912 (1980).
- [19] The KATRIN Collaboration, Nat. Phys. **18**, 160 (2022).
- [20] R. N. Mohapatra and A. Y. Smirnov, Ann. Rev. Nucl. Part. Sci. **56**, 569 (2006); R. N. Mohapatra, Nucl. Phys. B **908**, 423 (2016).
- [21] H. n. Li, Phys. Rev. D **107**, 054023 (2023).
- [22] H. n. Li, H. Umeeda, F. Xu and F. S. Yu, Phys. Lett. B **810**, 135802 (2020).
- [23] H. Y. Cheng, Phys. Rev. D **26**, 143 (1982).
- [24] A. J. Buras, W. Slominski and H. Steger, Nucl. Phys. **B245**, 369 (1984).
- [25] P. F. de Salas, D. V. Forero, C. A. Ternes, M. Tortola and J. W. F. Valle, Phys. Lett. B **782**, 633 (2018).
- [26] L. L. Chau and W. Y. Keung, Phys. Rev. Lett. **53**, 1802 (1984); L. Maiani, in Proceedings of the 1977 International Symposium on Lepton and Photon Interactions at High Energies (DESY, Hamburg, 1977), p. 867.
- [27] We have assumed that neutrinos are of the Dirac type to allow the existence of Fig. 3(b)